Electromechanical effects on tether formation from lipid membranes: A theoretical analysis

E. Glassinger, A. C. Lee, and R. M. Raphael
Department of Bioengineering, MS-142, Rice University, Houston, Texas 77251, USA
(Received 13 January 2005; revised manuscript received 18 May 2005; published 25 October 2005; publisher error corrected 24 January 2006)

The material properties of biomembranes can be measured by forming a tether, a thin bilayer tube that extends from the membrane surface. Recent experiments have demonstrated that the force required to maintain a tether is sensitive to the transmembrane potential. As a first approach towards understanding this phenomenon, a thermodynamic analysis of the influence of electrical fields on tether formation from an aspirated lipid vesicle is developed. The analysis considers contributions from Maxwell stresses as well as two forms of electromechanical coupling: coupling between the electric field and curvature strain (flexoelectric coupling) and between the electric field and areal strain (piezoelectric coupling). Predictions of equilibrium tether conformations are obtained numerically. For expected values of the dimensionless coupling parameters, flexoelectric coupling alters the force required to form a tether of a given length, while piezoelectric coupling and Maxwell forces do not greatly change the force versus tether length behavior. The results of this analysis indicate that tether experiments have the potential to characterize electromechanical coupling in both synthetic and cellular membranes.

DOI: 10.1103/PhysRevE.72.041926 PACS number(s): 87.16.Dg, 87.16.Ac, 87.10.+e

I. INTRODUCTION

Lipid membranes serve as a crucial component of many fundamental cellular processes such as endocytosis, intracellular trafficking, signaling, and division. Because these processes involve extensive lipid bilayer deformations, many basic advancements in biology and ultimately medicine depend upon understanding how lipid membranes respond to changes in mechanical, chemical, and electrical environments. This understanding can also aid in the development and implementation of biocompatible nanoelectromechanical systems.

One method to characterize the mechanical properties of lipid bilayers is to analyze the equilibrium conformation of a long, thin bilayer tube formed from the membrane surface. This tube, termed a tether, is created by pulling an attached silica bead away from the bilayer surface. The resulting tether length and radius depend upon the applied force as well as the membrane tension and material properties [1–3]. Analyses of tether experiments have provided sensitive measurements of the local bending stiffness of the membrane [1,2,4–6]. The local bending stiffness reflects the resistance of each monolayer to curvature changes. In addition, tether experiments have provided a quantitative confirmation of the area difference elasticity theory [1,2,5,7,8]. According to this theory, if the constituents of each monolayer redistribute to relieve local strains, curvature deformations lead to a relative tension difference between the two leaflets [9–11]. The modulus associated with this form of elasticity is the nonlocal bending stiffness.

Models of tether formation from aspirated, synthetic bilayers provide a foundation for the interpretation of tether formation experiments on cellular membranes. Tether experiments have characterized a number of material properties of cellular membranes such as the bending stiffness, apparent tension, and membrane-cytoskeleton adhesion energy [3,12–14]. As cells maintain a transmembrane potential and also possess an asymmetric distribution of charged lipids and proteins, determining how electrical fields affect tether conformation will help to characterize the electromechanical properties of cellular membranes. For example, the protein prestin, found in cochlear outer hair cells, imparts unique electromechanical properties to cellular membranes [15]. In recent experiments, the voltage clamp technique has been combined with optical tweezers to control the transmembrane potential during tether formation from cellular membranes. These experiments revealed that in prestin-transfected human embryonic kidney cells the tether force depends upon the holding potential [16].

A full interpretation of these results requires an understanding of how different electromechanical phenomena contribute to equilibrium tether conformations. The influence of applied electric fields on tether equilibrium has not been considered theoretically. Applied electric potentials may alter membrane conformation by a number of mechanisms including electrocompression and electromechanical coupling.

Applied charges compress the membrane and thus change membrane tension. The electrocompressive tension due to an applied voltage is derived from the Maxwell stress tensor and is proportional to the specific membrane capacitance C_m [17]. Maxwell stresses describe deformation of lipid vesicles in electric fields greater than typical physiological values [18,19].

Distinct from electrocompressive forces which depend upon the square of the applied field, electromechanical coupling phenomena depend upon an odd power of the field. One form of electromechanical coupling, flexoelectricity, occurs in asymmetric liquid crystalline materials [20]; experimental evidence suggests lipid bilayer membranes also exhibit this phenomenon [21,22]. According to this theory, altering the curvature or transmembrane potential creates a dipole or monopole (charge) asymmetry. Consequently, bending a bilayer changes the membrane polarization [21,23,24]; conversely, changing the applied field changes

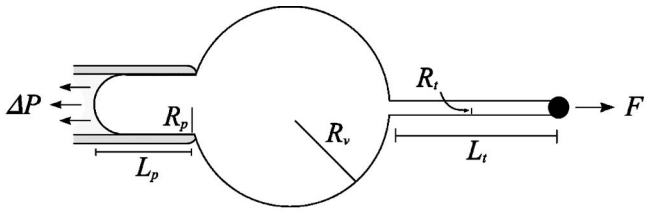

FIG. 1. Tether formation from an aspirated vesicle.

the membrane curvature [21]. Since curvature creates a material asymmetry, both symmetric and asymmetric bilayers are predicted to exhibit flexoelectricity [21,23,25]. In addition, asymmetric bilayers are predicted to manifest piezoelectricity, coupling between areal strain and the applied field [21].

To determine how these phenomena affect tether conformation, the energies of flexoelectric and piezoelectric coupling have been included in a thermodynamic analysis of tether formation from an aspirated vesicle. The contributions due to electrocompressive tensions are considered as well. We have chosen to analyze the aspirated vesicle because it is a simple, well-studied system [1,7]. The analysis indicates tether formation experiments may provide a novel method to test and characterize membrane electromechanical properties.

II. MODEL

In the experiment analyzed, a giant unilamellar vesicle is aspirated by a micropipette. Aspiration modulates the membrane tension and reduces the extent of the thermal undulations [26]. We consider a conceptual scenario in which the transmembrane potential can be controlled, possibly by inserting an electrode into a pipette containing a membrane perforator such as nystatin [27–29]. To form the tether, a force F is applied to the opposite side of the vesicle by an optical or magnetic force transducer. The aspirated vesicle-tether region is the system, and work is done at the boundaries via pressure in the pipette, the applied force, and the applied electric field.

Because the tether length-to-diameter ratio is large, the transmembrane potential may decrease along the tether. The decrease in potential estimated using a time-independent solution of the cable equation for a core conductor. If the vesicle contains a small amount of internal electrolyte ($\sim$5 mM), the calculated potential attenuation along a 200 μm tether is approximately 5% (see the Appendix). Smaller decreases are predicted for typical values of cellular membrane conductance and cytoplasmic resistivity. Given these results, the electric potential will be considered independent of length for tethers less than 200 μm long.

Following an approach developed by Božič *et al.* [7], the vesicle shape is parametrized into three regions: a cylindrical pipette projection of length L_p and radius R_p, a spherical vesicle of radius R_v, and a cylindrical tether of length L_t and radius R_t (Fig. 1). The end of the projection length is approximated as a cylindrical cap of radius R_p.

The total area is approximated as

$$A = -\pi R_p^2 + 2\pi L_p R_p + 4\pi R_v^2 + 2\pi L_t R_t. \tag{1}$$

The first term of Eq. (1) approximates the shared surface area at the intersection of the cylinder and sphere. Given $R_t \ll R_v$, the volume of the tether may be neglected and the total volume expressed as [7]

$$V = -\frac{\pi}{3}R_p^3 + \pi L_p R_p + \frac{4\pi}{3}R_v^3. \tag{2}$$

where the first term is the difference between the volume of a cylinder of length L_p and a hemispherical cap of radius R_p. To account for excess surface area, the parameter v is introduced to relate the volume to the surface area of the vesicle, $v = 3V_0/4\pi R^3$ where $A_0 = 4\pi R^2$. Under a constant volume constraint ($V = V_0$), the projection length can be expressed in terms of the vesicle radius [7]:

$$L_p = \frac{1}{\pi R_p^2}\left(V_0 + \frac{\pi}{3}R_p^3 - \frac{4\pi}{3}R_v^3\right). \tag{3}$$

In previous analyses, a constant-area constraint with a Lagrange multiplier proportional to the area expansivity modulus was used [7,30,31]. Since electrically induced tensions may alter membrane area, we have relaxed this constraint.

Equilibrium conformations are predicted by determining the stability points of the extended energy variational, $\delta\Pi = \delta G - \delta W$ [32,33]. For isothermal deformations, G is the electric Gibbs energy and W accounts for the external mechanical and electrical loads applied to the vesicle. Equilibrium tether conformations satisfy the following variational equation: $\delta G - \delta W = 0$. From the principles of virtual work,

$$W = FL_t + \Delta P \pi R_p^2 L, \tag{4}$$

where F is the tether force and ΔP is the aspiration pressure.

In the original tether experiments on aspirated vesicles, the aspiration pressure in the pipette was varied while the force was held constant [7]. Since later experimental advancements permitted the force to be varied as well [4], equilibrium predictions for both experimental cases are considered in this analysis.

For isothermal deformations, the electric Gibbs energy density (J/m^2) of a lipid bilayer is

$$\tilde{G} = \frac{1}{2}\kappa\alpha^2 + \frac{1}{2}k_c\bar{c}^2 + \frac{1}{2}\frac{k_r}{d^2}(\Delta A - \Delta A_0)^2 + \tilde{G}_E. \tag{5}$$

The first term is the bilayer area dilation energy density where κ is the area expansivity modulus and α is the percent change in the total area $[(A - A_0)/A_0]$.

The second term of Eq. (5), the local bending energy density, accounts for each individual monolayer's resistance to a change in curvature, $\bar{c}$. Because the curvature of the tether is much larger than any other region of the vesicle, this term is only integrated over the tether area [7]. Under this condition, $\bar{c} = 1/R_t$.

The third term of Eq. (5) is the nonlocal bending energy density that arises from area-difference elasticity. Here, k_r is the nonlocal bending modulus and d is the separation distance between the neutral surfaces of the two monolayers

[10,11]. For tether formation, the relative area difference ΔA is estimated from the difference between the area of the inner $[2\pi L_t(R_t-d/2)]$ and outer tether leaflets $[2\pi L_t(R_t+d/2)]$. Applying these approximations, the nonlocal bending energy becomes $2\pi^2 k_r(L_t-L_t^*)^2/A_0$. The parameter L_t^* is included to account for a possible initial area difference between the leaflets [1,7]. For this analysis, $L_t^*=0$.

The final term of Eq. (5) includes the energy densities of flexoelectric and piezoelectric coupling as well as the electric field energy density:

$$\tilde{G}_E = -f\bar{c}E - eE\alpha - \frac{1}{2}h\varepsilon\varepsilon_0 E^2. \tag{6}$$

Here f is the flexoelectric coupling coefficient, e is the piezoelectric coupling coefficient, $\varepsilon\varepsilon_0$ is the dielectric constant of the bilayer times the permittivity of free space, E is the membrane electric field, and h is the membrane thickness. Given that the tether curvature is several orders of magnitude larger than the other regions of the vesicle, the flexoelectric energy is integrated only over the tether area. Multiplying the final term of Eq. (6) by the total bilayer area provides the energy due to electrocompression of the bilayer [17,34]. The contributions of each of these three terms to equilibrium tether conformation are considered separately.

Integrating the energies of Eq. (5) over the appropriate area provides an expression for the full variational in terms of L_t, R_t, R_v, and E:

$$\Pi = \frac{1}{2}\kappa\frac{(A-A_0)^2}{A_0} + \pi k_c\frac{L_t}{R_t} + 2\pi^2 k_r\frac{(L_t-L_t^*)^2}{A_0} - eE(A-A_0) - 2\pi fEL_t - \frac{1}{2}h\varepsilon\varepsilon_0 E^2 A - FL_t - \Delta P\pi R_p^2 L_2. \tag{7}$$

It is instructive to express Eq. (7) in dimensionless form. For a characteristic length $R=\sqrt{A_0/4\pi}$ and an energy scale determined by the bending energy of a sphere $(8\pi k_c)$ [35], Eq. (7) becomes

$$\tilde{\Pi} = \frac{\kappa R^2}{4k_c}(a-1)^2 + \frac{1}{8}\frac{l_t}{r_t} + \frac{1}{16}\frac{k_r}{k_c}(l_t-l_t^*)^2 - \mathcal{E}_p(a-1) - \mathcal{E}_f l_t - \mathcal{E}_M^2 a - \mathcal{F}l_t - \Delta p r_p^2 l_p, \tag{8}$$

where the dimensionless area $a\,(A/4\pi R^2)$ is expressed in terms of the dimensionless tether-vesicle variables ($l_t=L_t/R$, $r_t=R_t/R$, $r_v=R_v/R$, $l_p=L_p/R$, and $r_p=R_p/R$): $a=r_v^2+r_t l_t/2+l_p r_p/2-r_p^2/4-1$. Note for the length scale chosen, $a_0=1$. The piezoelectric and flexoelectric coupling and Maxwell force parameters are, respectively,

$$\mathcal{E}_p = \frac{eR^2}{2k_c}E, \quad \mathcal{E}_f = \frac{fR}{4k_c}E, \quad \mathcal{E}_M = RE\sqrt{\frac{h\varepsilon\varepsilon_0}{4k_c}}.$$

The dimensionless mechanical force and pressure are

$$\mathcal{F} = \frac{FR}{8\pi k_c}, \quad \Delta p = \frac{\Delta P R^3}{8k_c}.$$

Equilibrium tether conformations for a given field E can be predicted by finding the stability points of Eq. (7) or (8). At a stability point, the first partial derivatives of Eq. (8) taken with respect to l_t, r_t, and r_v are equal to zero $[\partial\Pi(l_t,r_t,r_v)=0]$. This provides the following system of equations which can be solved to determine equilibrium tether conformations:

$$\frac{\partial\tilde{\Pi}}{\partial l_t} = \left[\frac{\kappa R_s^2}{k_c 2}(a-1) - \mathcal{E}_p - \mathcal{E}_M^2\right]\frac{r_t}{2} + \frac{1}{8r_t} + \frac{1}{8}\frac{k_r}{k_c}(l_t-l_t^*) - \mathcal{E}_f - \mathcal{F} = 0, \tag{9a}$$

$$\frac{\partial\tilde{\Pi}}{\partial r_t} = \left[\frac{\kappa R_s^2}{k_c 4}(a-1) - \mathcal{E}_p - \mathcal{E}_M^2\right]\left(\frac{l_t}{2}\right) - \frac{1}{8}\frac{l_t}{r_t^2} = 0, \tag{9b}$$

$$\frac{\partial\tilde{\Pi}}{\partial r_v} = \left(\frac{\kappa R_s^2}{k_c 4}(a-1) - \mathcal{E}_p - \mathcal{E}_M^2\right)\left(2r_v - \frac{2r_v^2}{r_p}\right) + 4r_v^2\Delta p = 0. \tag{9c}$$

Solutions were obtained numerically using a modified quasilinearization algorithm, a variant of the Newton-Raphson method in which the step size is adjusted iteratively by bisection to ensure the error is reduced [36,37].

Including electromechanical energies into the thermodynamic analysis modifies the equations derived in previous analyses of tether equilibrium [7]. The contribution of flexoelectric coupling to the tether force can be determined by combining the dimensional form of Eqs. (9a) and (9b):

$$F_{eff} = \frac{2\pi k_c}{R_t} + \frac{4\pi^2 k_r L_t}{A_0}. \tag{10}$$

Inclusion of the flexoelectric coupling energy adds a new term to the effective force F_{eff} previously defined [7]: $F_{eff}(E)=F+4\pi k_r L_t^*/A_0+2\pi fE$. Coupling between membrane curvature and the electric field shifts the mechanical force F needed to maintain a tether of a given length by $2\pi fE$.

The contributions of piezoelectric coupling and Maxwell forces to tether equilibrium become apparent upon rearrangement of Eq. (9c) in dimensional form:

$$\bar{T} = \frac{R_v\Delta P}{2}\frac{R_p}{(R_v-R_p)} + \frac{1}{2}h\varepsilon\varepsilon_0 E^2. \tag{11}$$

Here the isotropic tension $\bar{T}$ satisfies the thermodynamic relation: $\bar{T}=\partial\tilde{G}/\partial\alpha=\kappa\alpha-eE$. Equation (11) is of the same form as the equation for the tension of an aspirated vesicle; piezoelectric coupling modifies the tension term on the left-hand side and Maxwell forces contribute to the applied load on the right-hand side [38].

Here, we investigate how the effective electromechanical parameters alter tether conformation. The model is applied to the two experimental conditions mentioned earlier: constant force and constant pressure.

III. RESULTS

Equilibrium tether conformations were determined for typical vesicle dimensions and membrane material parameters. The following values were used for all calcula-

tions: $\kappa=0.180$ N/m, $k_c=1.0\times10^{-19}$ J, $k_r=3.6\times10^{-19}$ J, $A_0=4\pi\times10^{-10}$ m^2, $\upsilon=0.75$, and $R_p=3.5$ μm. To determine the extent area expansivity changes equilibrium tether conformation, the numerical results in which $E=0$ are compared to the solutions in which the constant area constraint was applied. The differences due to area expansion are not large enough to be discerned experimentally. These results support the constant area approximation applied in previous tether analyses [1,7,30,39].

To determine the relative contributions of each form of electromechanical energy, plots are provided in dimensionless form. For both experimental conditions, the contribution of all three electromechanical parameters to either the equilibrium force or pressure required to maintain the tether at a constant length is determined. In addition, the relationship between l_p and l_t is plotted for several values of each dimensionless electromechanical parameter. For a membrane under voltage clamp, the values of the electromechanical parameters are calculated under the boundary condition $E=\phi/h$ where h is the membrane thickness (5 nm) and ϕ is the applied potential. This condition has been applied for previous calculations of the converse flexoelectric coefficient of lipid bilayers [24] and the piezoelectric coefficient of the outer hair cell membrane [40]. For all three electromechanical parameters, dimensional plots are also included as specific experimentally relevant examples. In these plots, the dependence of the tether length on the applied force and transmembrane potential is provided.

A. Maxwell forces

To determine how Maxwell forces affect tether conformation, the electrocompressive energy was introduced into the Gibbs energy density. For typical values of the specific membrane capacitance ($\varepsilon\varepsilon_0/h\leqslant1$ μF/cm^2), no significant changes in tether conformation are predicted for values of $\mathcal{E}_m$ which span physiologically relevant potentials. The contribution of $\mathcal{E}_m$ to tether conformation is shown in Figs. 2 and 3. When $\mathcal{E}_m$ is increased from 0 to 1000, l_p increases by 5% in both experimental cases. In the constant-pressure case, $\mathcal{F}$ increases by less than 1% [Fig. 2(A)] and similarly, in the constant force condition, Δp decreases by less than 2% [Fig. 2(C)]. The plots in Fig. 2 show the dependence of $\mathcal{F}$ on $\mathcal{E}_m$ for tethers of different fixed lengths. In Fig. 3(A), a dimensional plot of the dependence of tether length of both φ and F is given.

B. Flexoelectric coupling

To determine the extent to which flexoelectric effects influence tether behavior, the coupling energy was introduced into the electric Gibbs energy density. Minimization of Eq. (8) indicates that coupling coefficients on the order of those measured for lipid bilayers can affect tether conformation [Fig. 3(B)]. For a vesicle with a typical flexoelectric coefficient of 2×10^{-19} C [21] under a 100-mV potential, the dimensionless flexoelectric parameter $\mathcal{E}_f$ is 10. For coupling parameters of this magnitude, flexoelectric coupling changes the force required to form a tether of a given length [Fig. 4(A)]. For the constant-pressure case, the coupling does not significantly alter the relation between the l_p and l_t [Fig. 4(B)]. Experimentally, this relation is used to calculate the tether radius [1]. The predictions for the constant force tether formation case are given in Figs. 4(C) and 4(D). In this case, flexoelectric coupling alters the pressure required to maintain a tether of a given length. The differences in the slopes of l_p vs l_t curves reflect different tether radii arising from the different aspiration pressures. A dimensional example of the dependence of the tether length on the tether force and applied potential is also provided in Fig. 3(B).

C. Piezoelectric coupling

Inclusion of the piezoelectric coupling energy into Eq. (8) alters the predicted equilibrium tether conformation for both experimental conditions. For a bilayer with a bending stiffness of 1.0×10^{-19} J and an expected piezocoefficient of 10^{-12} C/m [25], the dimensionless coupling parameter $\mathcal{E}_p$ for a 100-mV transmembrane potential is 10^4. For a piezoelectric coupling parameter of this magnitude, virtually no change in tether force is predicted [Figs. 3(C) and 5(A)]. If $\mathcal{E}_p$ is increased by two orders of magnitude (10^6), small, but observable, changes in tether force and aspiration pressure are predicted [Figs. 5(A) and 5(C)]. For both constant-force and constant-pressure conditions, the coupling parameter changes l_p [Figs. 5(B) and 5(D)] but does not alter the slope of l_p vs l_t.

IV. DISCUSSION

Inclusion of the electromechanical energies into the thermodynamic potential of tether formation changes the predicted minimum-energy conformation. The extent of the change in tether conformation depends upon the magnitude of the coefficient and the type of coupling considered. For typical values of the membrane capacitance and transmembrane potentials within a physiological range, electrocompressive effects do not greatly change the minimum-energy tether conformation. Experimentally discernable effects are predicted for flexoelectric parameters which span previously measured values of f. Only piezoelectric coupling parameters which correspond to large values of e ($>10^{-10}$ C/m) are expected to lead to observable changes in tether conformation.

The manner in which the two forms of coupling affect tether conformation is reflected by the thermodynamic constitutive relationships for membrane tension and bending moment. Flexoelectric coupling alters the membrane bending moment M: $M=k_c\bar{c}+k_r\alpha_\pm/h-fE$ [25,41]. Since the tether force is $2\pi M$ [6,42], the change in equilibrium tether force reflects the flexoelectric contributions to the bending moment. Piezoelectric coupling, on the other hand, changes the relationship between area expansion and membrane tension: $T=\kappa\alpha-eE$. Because the pipette aspiration pressure controls the membrane tension, piezoelectric coupling will lead to changes in membrane area. For a fixed-tension case such as the one considered in this paper, piezoelectric coupling is not expected to greatly change the tether force. Although large piezoelectric parameters can theoretically lead to small

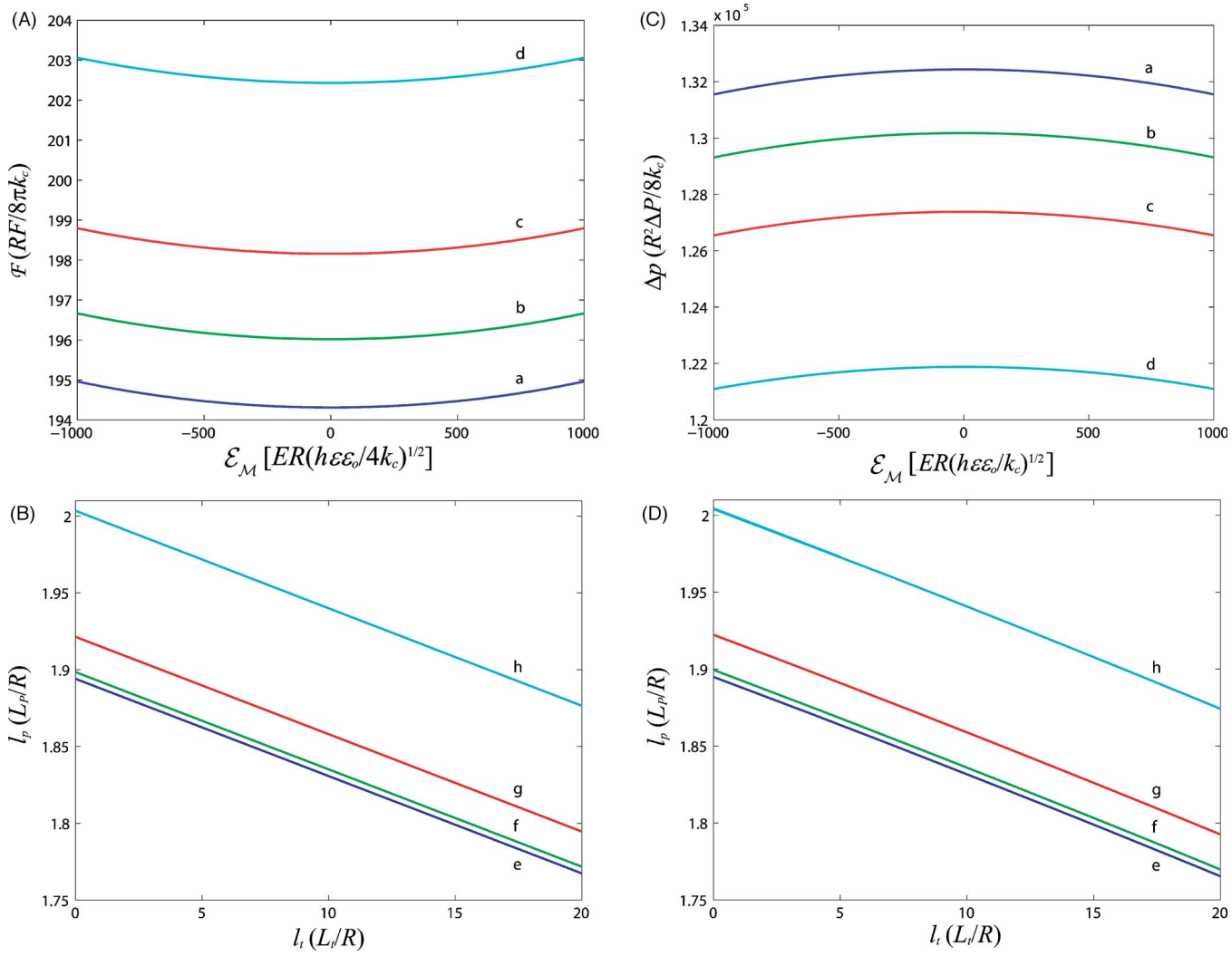

FIG. 2. (Color online) Maxwell forces are predicted to have little effect on tether formation for both constant pressure and force conditions. For the constant-pressure case [plots (A) and (B)], $\Delta p = 1.25 \times 10^5$; for the constant-force case [plots (C) and (D)], $\mathcal{F} = 200$. The dependence of the force and pressure on the value of $\mathcal{E}_m$ is plotted for four values of l_t: (a) 1, (b) 5, (c) 10, and (d) 20. Changing the value of $\mathcal{E}_m$ does not appreciably alter the slope of the l_p vs l_t curves [plots (B) and (D)]. For these plots, the values of $\mathcal{E}_m$ are (e) 0, (f) 200, (g) 500, and (h) 1000.

changes in tether force (Fig. 5), the accompanying areal expansion allows the contributions of a large piezoelectric parameter to be distinguished from those of a small flexoelectric parameter (Figs. 4 and 5). Since analyses of tether experiments conducted on cellular membranes rely upon models of synthetic systems, this analysis provides a theoretical foundation towards understanding how different electromechanical phenomena affect tether conformation.

The most interesting result of this analysis is that flexoelectricity can potentially have a discernible effect on tether conformation. Previous measurements of the flexoelectric coefficient have been conducted on black lipid membranes and membrane patches [22]. For these experiments, the radius of curvature is typically on the order of ~ 5 μm. Since equilibrium tether radii are at least an order of magnitude smaller, tether formation can provide a new method to explore the effects of flexoelectric coupling on highly curved biological structures. Since the predicted equilibrium tether length is sensitive to flexoelectric energy, tether experiments should provide an ideal test of the flexoelectric hypothesis.

The magnitude of the flexoelectric coefficient of a membrane depends upon membrane composition as well as the frequency of the applied stimulation. When a bilayer membrane bends, the outer leaflet expands and the inner leaflet compresses. The resulting differential density of the two leaflets relaxes by mechanically driven slip opposed by viscous dissipation at the bilayer midplane [2,5]. Under high-frequency changes in either curvature or applied field, the differential density may not fully relax. Thus, the membrane will bend as if the two leaflets were connected to each other. Depending upon the lipid species, the coefficients range in magnitude from 10^{-20} to 10^{-18} C for frequency changes greater than 200–300 Hz [21]. For lower-frequency stimulations, the lipids have more time to diffuse into or out of the curved region to relieve the local differential density induced by bending. Since each individual monolayer will bend around its own neutral surface rather than the bilayer neutral surface, the coupling coefficients for lower-frequency stimu-

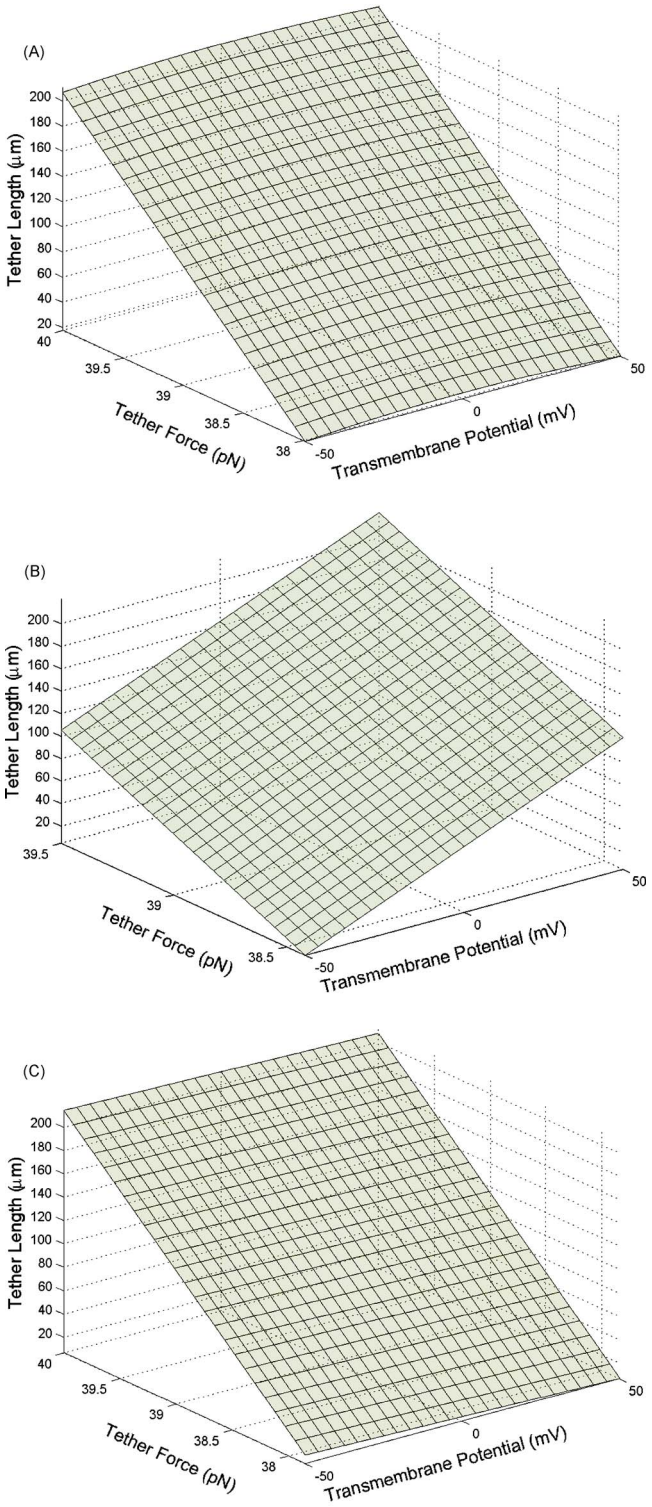

FIG. 3. (Color online) Influence of (A) Maxwell forces ($C_m = 100\ \mu F/cm^2$), (B) flexoelectric ($f = 10^{-20}$ C), and (C) piezoelectric coupling ($e = 10^{-10}$ C/m) on the tether length for a range of transmembrane potentials and tether forces. The simulations are for the constant-pressure experimental condition in which $\Delta P = 60$ Pa. Note that large values of C_m and e are chosen to show the trends for Maxwell forces and piezoelectricity.

lations are less than those of higher frequencies [21]. This implies that applying high-frequency voltage stimulation will enhance the flexoelectric response of a membrane tether.

Because cellular membranes are composed of an asymmetric distribution of charged lipids and polar proteins, the flexocoefficients can be quite large. The high-frequency coefficients of a patch of locust muscle membrane, for example, are on the order of 10^{-18} C [21]. For a coefficient of this magnitude, lower-frequency stimulations should affect tether conformation. In fact, tethers formed from prestin-transfected HEK cells exhibit voltage sensitivity during dc stimulation [16].

Charge and dipole asymmetries are expected to confer piezoelectric properties to cellular membranes. From monolayer measurements, the piezoelectric coefficient of lipid bilayers is estimated to be of the order of 10^{-12} C/m [21]. This is too small to cause measureable changes in the tether-vesicle conformation. Just as for flexoelectric effects, integral membrane proteins could potentially increase the piezoelectric modulus.

One protein which augments membrane electromechanical coupling properties is prestin. This unique integral membrane protein is responsible for the voltage-dependent length changes and signature nonlinear capacitance of outer hair cells [15,43]. The outer hair cell electromotile response amplifies the motion of the basilar membrane and is required for normal auditory sensation. How prestin confers electromotility to the membrane is a subject of active debate. A number of theories describe voltage-induced changes in cell length using both linear and nonlinear piezoelectric-type approaches [44–54]. Macroscale analysis of the whole-cell deformation provides a linear piezoelectric coupling coefficient on the order of 10^{-3} N/V m [47,48]. Multiplied by the membrane thickness (5 nm), this is equivalent to a coupling coefficient of 10^{-12} C/m. Other models suggest that instead of expanding membrane area, prestin changes the membrane curvature via a flexoelectric mechanism [41]. For this model, a flexoelectric coefficient of 10^{-19} C is sufficient to explain whole-cell deformation. Currently, these two models can not be distinguished experimentally. As this current analysis indicates that the two forms of electromechanical coupling affect tether conformation differently, tether experiments may be used to explore the properties of electroactive proteins such as prestin. Determining the extent to which electromechanical phenomena affect membrane conformation will help to deepen understanding of the role of electrostatic forces in diverse cellular events.

ACKNOWLEDGMENTS

We express our sincere gratitude to Dr. Chad Landis for helpful discussions, Dr. William Brownell for his suggestions regarding the cable analysis, and Imran Quraishi for his assistance with the minimization routines. This work was supported by the National Science Foundation under Grant No. 0114264.

APPENDIX

Spatial attenuation of the transmembrane potential

Spatial attenuation of the transmembrane potential along a cylindrical core conductor can be described by the cable

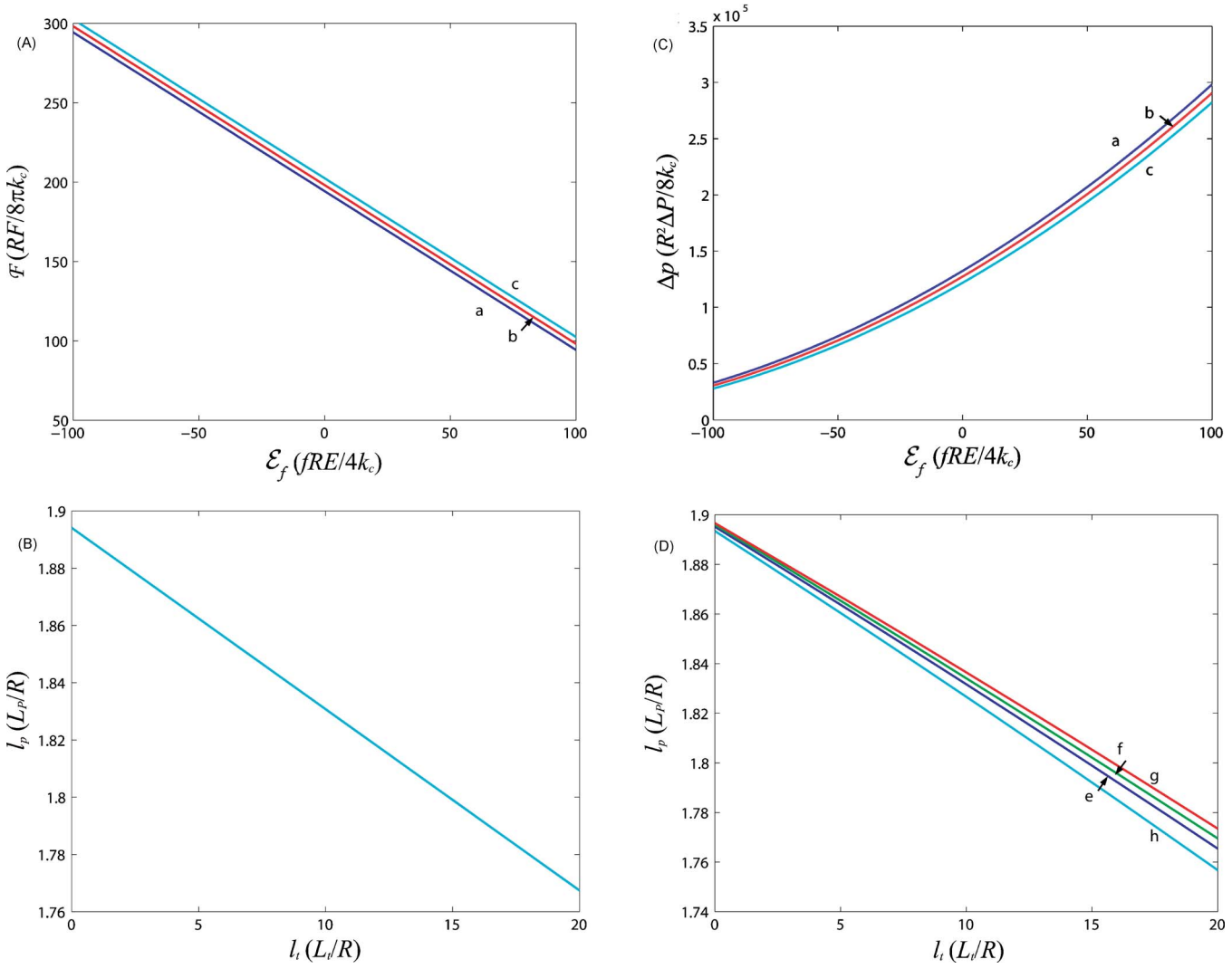

FIG. 4. (Color online) Numerical predictions of the influence of flexoelectic coupling on the conformation of tethers formed under two different conditions: constant pressure $\Delta p = 1.25 \times 10^5$ [(A) and (B)] and constant force $\mathcal{F} = 200$ [(C) and (D)]. The l_p vs l_t curves are plotted for four values of $\mathcal{E}_f$: (e) 0, (f) 1, (g) 10, and (h) −10. The dependence of the dimensionless force and pressure on the value of the $\mathcal{E}_f$ is plotted for three values of l_t: (a) 1, (b) 10, and (c) 20. Note that all three tether lengths are graphed in plot (B).

equation [55,56]. If the resistance per unit length of the outer conductor is much less than that of the inner conductor, the space constant can be approximated as

$$\lambda_C \cong \sqrt{a/2\rho_i G_m}, \tag{A1}$$

where ρ_i is the resistivity of the core of the conductor, G_m is the specific membrane conductance, and a is the radius of the cable. The conductance of synthetic lipid bilayers is small, typically on the order of 10^{-3} S/m^2 [57]. The resisitivity depends upon the electrolyte concentration inside of the vesicle. For 5 mM NaCl, the resisitivity is 17 Ω m [58]. Due to the interest in the electromechanical properties of the outer hair cell (OHC) membrane, we have also calculated the space constant for a tether formed from an OHC. The space constant is estimated using the specific conductance of the outer-hair-cell lateral wall ($G_m = 0.01$ S/m^2) and the cytoplasmic resistivity ($\rho_i = 0.070$ Ω m) [59]. Using these values, λ_C for a 10-nm radius tether is ~840 μm.

Semi-infinite cable

For a semi-infinite cable ($0 \leqslant z \leqslant +\infty$) in which no additional voltage or current is applied along its length and $v_m(0) = \phi$, the following unique solution holds [55]:

$$v_m(z) = \phi e^{-z/\lambda_C}. \tag{A2}$$

The semi-infinite cable approximation is valid for cables longer than 4 times the space constant. The spatial potential attenuation for a semi-infinite cable is plotted in Fig. 6.

Finite cable

If the length of the cable is less than $4\lambda_C$, then the length of the cable L and the boundary conditions at the end of the cable must be considered. If the end of the cable is sealed (i.e., negligible current flows though the end of the cable), then an open-circuit approximation may be applied, where $dv_m/dz = 0$ at $z = L$. For $v_m(0) = \phi$, a unique solution is

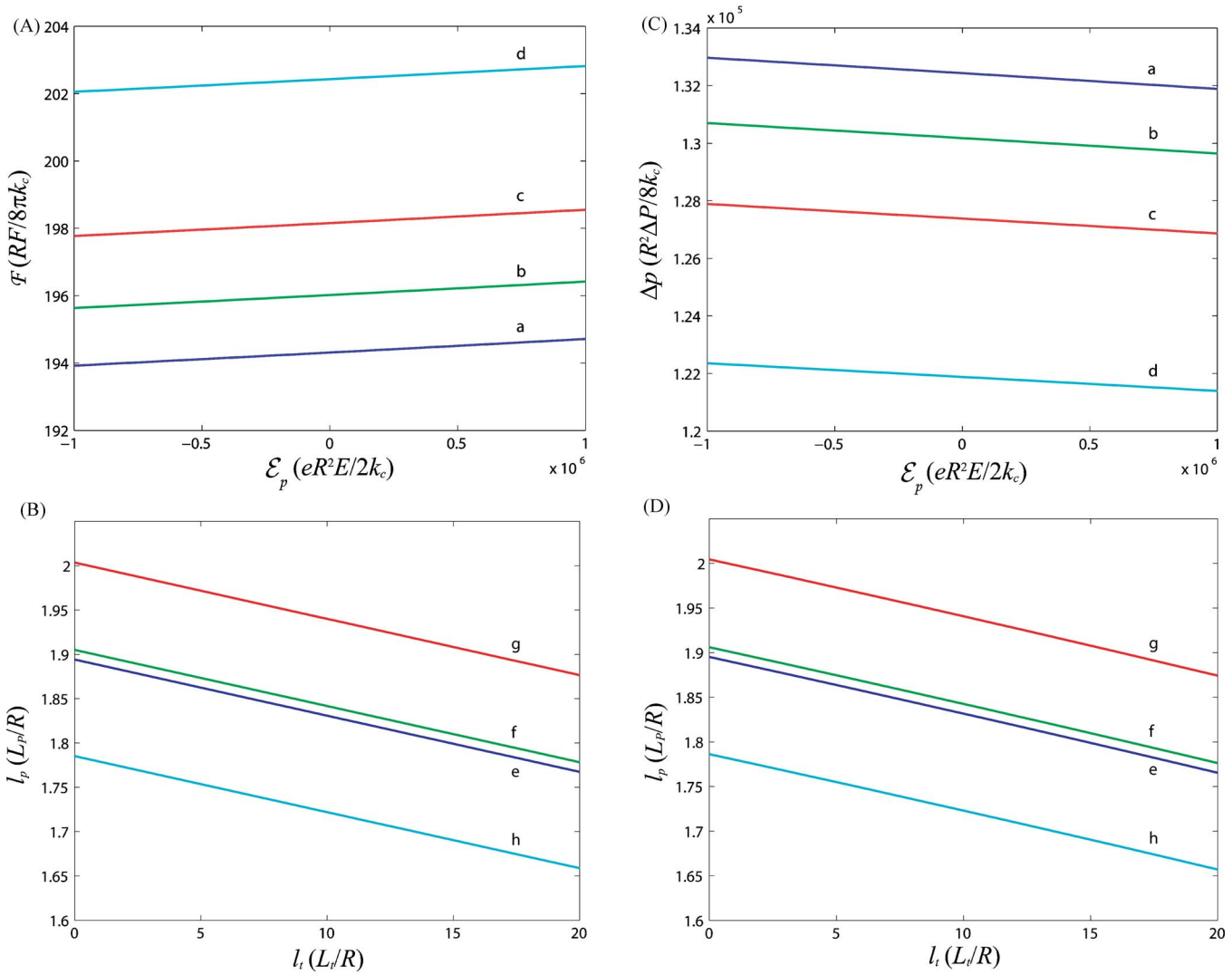

FIG. 5. (Color online) Numerical predictions of the influence of piezoelectric coupling on the conformation of tethers formed under constant pressure, $\Delta p = 1.25 \times 10^5$ [(A) and (B)] and constant-force conditions $\mathcal{F} = 200$ [(C) and (D)]. The dependence of the force and pressure on the value of the $\mathcal{E}_p$ is plotted for four values of l_t: (a) 1, (b) 5, (c) 10, and (d) 20. The values of $\mathcal{E}_p$ used in the l_p vs l_t plots are (e) 0, (f) 10^5, (g) 10^6, and (h) -10^{-6}.

$$v_m\left(\frac{z}{\lambda_C}\right) = \frac{\phi \cosh\left(\frac{L}{\lambda_C} - \frac{z}{\lambda_C}\right)}{\cosh\left(\frac{L}{\lambda_C}\right)}. \qquad \text{(A3)}$$

The potential decrease along the length of a finite cable is plotted in Fig. 6.

[1] R. E. Waugh, J. Song, S. Svetina, and B. Zeks, Biophys. J. **61**, 974 (1992).
[2] E. Evans and A. Yeung, Chem. Phys. Lipids **73**, 39 (1994).
[3] R. M. Hochmuth, J. Y. Shao, J. Dai, and M. P. Sheetz, Biophys. J. **70**, 358 (1996).
[4] V. Heinrich and R. E. Waugh, Ann. Biomed. Eng. **24**, 595 (1996).
[5] R. M. Raphael and R. E. Waugh, Biophys. J. **71**, 1374 (1996).
[6] R. E. Waugh and R. M. Hochmuth, Biophys. J. **52**, 391 (1987).
[7] B. Božič, S. Svetina, B. Zeks, and R. E. Waugh, Biophys. J. **61**, 963 (1992).

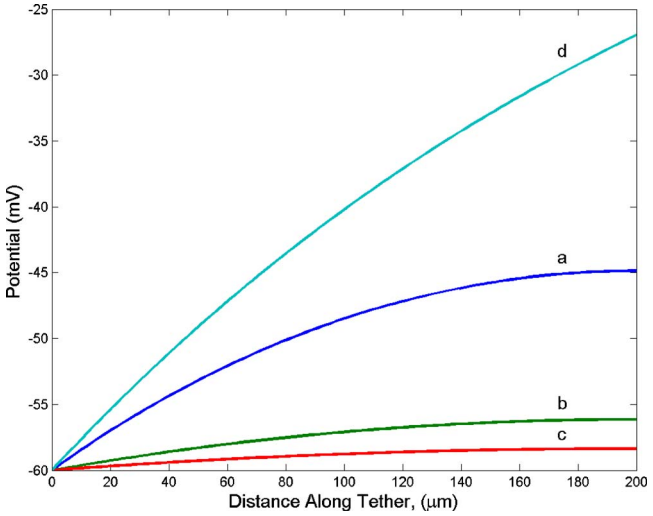

FIG. 6. (Color online) Spatial decay of potential along a finite and semi-infinite cable. The attenuation of the potential along a finite 200-μm cable is plotted for three values of the space constant. The space constants for a tether formed from a synthetic bilayer are (a) $\lambda_c=250$ μm for a NaCl concentration of 0.5 mM ($G_m=10^{-3}$ S/m^2, $\rho_i=16$ Ω m) and (b) $\lambda_c=542$ μm for a NaCl concentration of 5 mM ($G_m=10^{-3}$ S/m^2, $\rho_i=1.7$ Ω m). The estimated space constant for an outer hair cell tether is (c) 845 μm. The semi-infinite cable solution (d) is plotted for $\lambda_c=250$ μm. All space constants are calculated for a tether radius of 10 nm.

[8] D. J. Bukman, J. H. Yao, and M. Wortis, Phys. Rev. E **54**, 5463 (1996).
[9] L. Miao, U. Seifert, M. Wortis, and H. G. Dobereiner, Phys. Rev. E **49**, 5389 (1994).
[10] E. A. Evans, Biophys. J. **14**, 923 (1974).
[11] S. Svetina, M. Brumen, and B. Zeks, Stud. Biophys. **110**, 177 (1985).
[12] Z. Li *et al.*, Biophys. J. **82**, 1386 (2002).
[13] M. P. Sheetz, Nat. Rev. Mol. Cell Biol. **2**, 392 (2001).
[14] R. M. Hochmuth and W. D. Marcus, Biophys. J. **82**, 2964 (2002).
[15] J. Zheng *et al.*, Nature (London) **405**, 149 (2000).
[16] F. Qian, S. Ermilov, D. Murdock, W. E. Brownell, and B. Anvari, Rev. Sci. Instrum. **75**, 2937 (2004).
[17] J. Akinlaja and F. Sachs, Biophys. J. **75**, 247 (1998).
[18] A. Sokirko, V. Pastushenko, S. Svetina, and B. Zeks, Bioelectrochem. Bioenerg. **34**, 101 (1994).
[19] M. Kummrow and W. Helfrich, Phys. Rev. A **44**, 8356 (1991).
[20] R. Meyer, Phys. Rev. Lett. **22**, 918 (1969).
[21] A. Petrov, *The Lyotropic State of Matter: Molecular Physics and Living Matter Physics* (Gordon and Breach, Amsterdam, 1999), p. 549.
[22] K. Sun, J. Phys. Chem. B **101**, 6327 (1997).
[23] A. G. Petrov and V. S. Sokolov, Eur. Biophys. J. **13**, 139 (1986).
[24] A. T. Todorov, A. G. Petrov, and J. H. Fendler, J. Phys. Chem. **98**, 3076 (1994).
[25] A. Petrov, Biochim. Biophys. Acta **85535**, 1561 (2001).
[26] E. Evans and W. Rawicz, Phys. Rev. Lett. **64**, 2094 (1990).
[27] C. Katnik and R. Waugh, Biophys. J. **57**, 877 (1990).
[28] M. Goulian *et al.*, Biophys. J. **74**, 328 (1998).
[29] R. Horn and A. Marty, J. Gen. Physiol. **92**, 145 (1988).
[30] V. Heinrich, B. Bozic, S. Svetina, and B. Zeks, Biophys. J. **76**, 2056 (1999).
[31] B. Bozic, S. Svetina, and B. Zeks, Phys. Rev. E **55**, 5834 (1997).
[32] H. F. Tiersten, Proc. IEEE 55, 1523 (1967).
[33] A. Benjeddou, Comput. Struct. **76**, 347 (2000).
[34] D. Needham and R. M. Hochmuth, Biophys. J. **55**, 1001 (1989).
[35] S. Svetina and B. Zeks, Eur. Biophys. J. **17**, 101 (1989).
[36] S. C. Garg (unpublished).
[37] A. Miele and A. Levy (unpublished).
[38] R. Kwok and E. Evans, Biophys. J. **35**, 637 (1981).
[39] S. Svetina, B. Zeks, R. E. Waugh, and R. M. Raphael, Eur. Biophys. J. **27**, 197 (1998).
[40] A. A. Spector and R. P. Jean, J. Biomed. Eng. **126**, 17 (2004).
[41] R. M. Raphael, A. S. Popel, and W. E. Brownell, Biophys. J. **78**, 2844 (2000).
[42] A. Yeung and E. Evans, J. Phys. I **5**, 1501 (1995).
[43] M. C. Liberman *et al.*, Nature (London) **419**, 300 (2002).
[44] R. Hallworth, B. N. Evans, and P. Dallos, J. Neurophysiol. **70**, 549 (1993).
[45] P. Dallos, R. Hallworth, and B. N. Evans, J. Neurophysiol. **70**, 299 (1993).
[46] A. A. Spector, M. Ameen, and R. A. Schmiedt, Biomech. Model Mechanobiol. **1**, 123 (2002).
[47] J. A. Tolomeo and C. R. Steele, J. Acoust. Soc. Am. **97**, 3006 (1995).
[48] A. A. Spector, J. Acoust. Soc. Am. **107**, 1435 (2000).
[49] K. H. Iwasa, Biophys. J. **81**, 2495 (2001).
[50] A. A. Spector, M. Ameen, and A. S. Popel, Biophys. J. **81**, 11 (2001).
[51] A. Spector, Int. J. Solids Struct. **38**, 2115 (1999).
[52] W. E. Brownell, A. A. Spector, R. M. Raphael, and A. S. Popel, Annu. Rev. Biomed. Eng. **3**, 169 (2001).
[53] E. K. Weitzel, R. Tasker, and W. E. Brownell, J. Acoust. Soc. Am. **114**, 1462 (2003).
[54] N. Deo and K. Grosh, Biophys. J. **86**, 3519 (2004).
[55] T. Weiss, *Cellular Biophysics: Electric Properties of Cellular Membranes* (MIT Press, Cambridge, MA, 1996).
[56] W. Rall and H. Agmon-Snir, in *Methods in Neuronal Modeling*, edited by C. Koch and I. Segev (MIT Press, Cambridge, MA, 1998), pp. 27–40.
[57] M. Montal and P. Mueller, Proc. Natl. Acad. Sci. U.S.A. **69**, 3561 (1972).
[58] D. Lide, Ed., *Handbook of Chemistry and Physics*, 83rd ed., edited by D. Lide (CRC Press, Boca Raton, FL, 2002).
[59] J. A. Halter, R. P. Kruger, M. J. Yium, and W. E. Brownell, NeuroReport **8**, 2517 (1997).